Available online at www.sciencedirect.com

ScienceDirect

Energy Procedia 124 (2017) 842–850

Energy Procedia

www.elsevier.com/locate/procedia

7th International Conference on Silicon Photovoltaics, SiliconPV 2017

Contact resistivity reduction on lowly-doped n-type Si using a low workfunction metal and a thin TiO_X interfacial layer for doping-free Si solar cells

Jinyoun Cho[a,b]*, Maarten Debucquoy[b], Maria Recaman Payo[b], Shuja Malik[b], Miha Filipič[b], Hariharsudan Sivaramakrishnan Radhakrishnan[b], Twan Bearda[b], Ivan Gordon[b], Jozef Szlufcik[b], Jef Poortmans[a,b,c]

[a]*ESAT department, K.U. Leuven, Leuven B-3001, Belgium*
[b]*imec, Kapeldreef 75, Leuven B 3001, Belgium*
[c]*University Hasselt, Martelarenlaan 42, Hasselt 3500, Belgium*

Abstract

Eliminating a doping process could be an effective way to reduce the production cost of c-Si cells. However, in absence of highly doped Si, the formation of a high quality contact is not straightforward. The lack of field-effect passivation from a lowly doped region can lead to a high recombination current density at the contacts ($J_{0,metal}$) and moreover, contact resistivity (ρ_C) typically increases when doping level is decreasing. In this work we focus on reducing the contact resistivity of an electron-selective contact for doping-free cells. Although the effect of low work function metals (LWMs) in combination with an i-a-Si:H layer has already been reported, the synergy effect of a LWM and a MIS (Metal-Insulator-Semiconductor) contact structure on top of the i-a-Si:H has not been reported yet. Here, we demonstrate a new ATOM (i-**a**-Si:H / **T**iO_X / l**o**w workfunction **m**etal) contact structure as an electron-selective contact using an i-a-Si:H layer, a TiO_X interfacial layer and Ca (Φ = 2.9eV) without requiring an additional n^+ doping process. The addition of TiO_X in between the i-a-Si:H layer and the Ca decreases the ρ_C by about 2 orders of magnitude. Despite of increased $J_{0,metal}$ due to e-beam processing of TiO_X, the Ca based ATOM contact increases the potential max efficiency up to 25 %. To the best of our knowledge, this is the first demonstration of an electron-selective contact comprising a low work function metal, an interfacial TiO_X and an i-a-Si:H passivation layer. This type of contact could be a promising route for the optimization of doping-free cells

Peer review by the scientific conference committee of SiliconPV 2017 under responsibility of PSE AG.

Keywords: Contact resistivity; MIS; Low workfunction metal; Titanium oxide; carrier selective contact

* Corresponding author. Tel.: +32 484 62 41 04

1876-6102
Peer review by the scientific conference committee of SiliconPV 2017 under responsibility of PSE AG.
10.1016/j.egypro.2017.09.356

E-mail address: jinyoun.cho@imec.be

1. Introduction

The importance of cost reduction and performance increase has only grown since average PV module prices (€/W_P) have dropped sharply over the last decade [1]. Process simplification can be an option to lower the production cost. As each doping process (ex. tube thermal diffusion, ion-implantation) is accompanied by pre- and post-cleaning steps, the elimination of a doping process could be a very effective way to reduce cell production cost. In absence of a doping process, the contacts themselves need to be carrier-selective to be able to guide the light-generated electrons and holes to the opposite contacts. However, making a good contact on a lowly doped surface is very challenging due to the weak field-effect passivation and the high contact resistivity. Possible candidates to decrease the contact resistivity on a lowly doped n-type layer are low workfunction metals (LWMs) and carrier-selective MIS (Metal-Insulator-Semiconductor) contacts. On one hand, LWMs tend to form a low Schottky barrier for the electrons, although metal fermi level ($E_{F,metal}$) pinning might hinder the reduction of this Schottky barrier (see Fig. 1. (a)) [2]. In MIS contacts on the other hand, the insulator can effectively reduce the $E_{F,metal}$ pinning, allowing lower Schottky barriers and effectively reducing contact resistivity for lowly doped surfaces, in comparison to MS (Metal-Semiconductor) contacts [3,4].

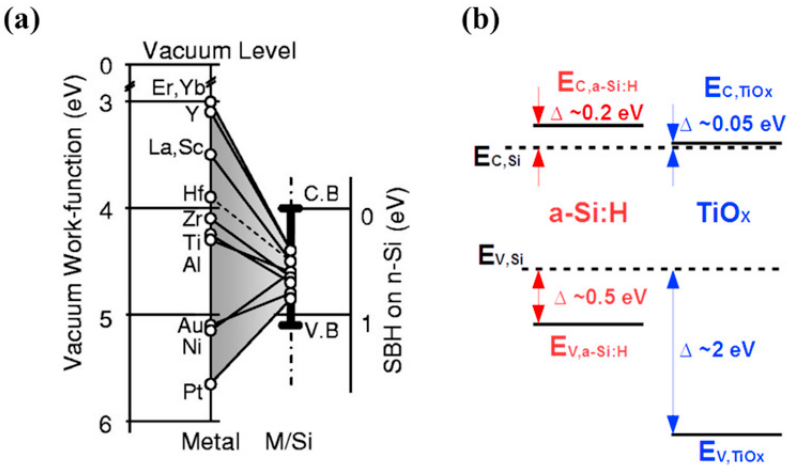

Fig. 1. (a) Metal fermi level pinning position in n-Si. (b) Typical energy band structure of a-Si:H and TiO_X relative to c-Si

Bullock et al. presented a doping-free silicon solar cell, which comprised a LWM equivalent structure (LiF/Al, Φ = 2.9 eV) on an intrinsic a-Si:H (i-a-Si:H) passivation layer to take an advantage of the LWM for the electron-selective contact [5]. And Allen et al. demonstrated ohmic Calcium (Φ = 2.9 eV) contact on a bare n-type silicon wafer without additional n+ doping [6]. However, a synergy effect of a LWM and a MIS structure on a-Si:H passivation layer has not been reported yet, despite the fact that i-a-Si:H causes similar $E_{F,metal}$ pinning effects to c-Si [7]. In particular, TiO_X stands out as a promising interfacial layer for an MIS electron-selective contact due to the small conduction band offset relative to Si (see Fig. 1. (b)), which results in a low tunneling resistance [8,9].

In this study, we demonstrate a novel Ca based ATOM (i-**a**-Si:H / **T**iO_X / l**o**w workfunction **m**etal) contact structure, which is a Ca and a TiO_X interfacial layer on top of an i-a-Si:H passivated n-type silicon Cz wafer without n+ doping. Effects of metal work function and TiO_X interfacial layer are studied.

2. Experiment

Chemically polished n-type Cz wafers ((100), 2.6 Ω·cm, 186 μm) were used. After wafer cleaning, intrinsic a-Si:H layers of various thicknesses were deposited on both sides of the substrates by plasma enhanced chemical

vapor deposition (PECVD). Wafers were diced to squares of 54 x 54 mm^2 (for recombination current density in the metallized area, $J_{0,metal}$) and 30 x 30 mm^2 (for contact resistivity, ρ_C). On top of the i-a-Si:H, a TiO_X layer was grown by e-beam evaporation. A Ca/Al stack formed by thermal evaporation completed the electron-selective contact. Two different test structures were fabricated to measure $J_{0,metal}$ and ρ_C (see Fig. 2).

For the measurement of $J_{0,metal}$, blanket thin layers of 4 nm Ca and 6 nm Al were deposited only at the rear-side and minority carrier lifetime was measured by the quasi-steady-state-photo-conductance method (QSSPC). Since fitting J_0 at a high level injection (excess carrier density > 1e16 cm^{-3}) [10] was not good, $J_{0,metal}$ was calculated by equations (1)-(2). $J_{0,front}$ is regarded as a same J_0 measured before Ca/Al evaporation. $J_{0,bulk}$ was of about 10 fA/cm^2(the difference between Cz wafer and FZ wafer). J_{SC} of 36 mA/cm^2 (typical J_{SC} of our SHJ solar cells) and kT/q of 25.9 mV were used for the $J_{0,total}$ calculation.

$$iV_{OC} = \left(\frac{kT}{q}\right)\ln\left(\frac{J_{SC}}{J_{0,total}} + 1\right) \tag{1}$$

$$J_{0,total\ after\ Ca/Al} = J_{0,front} + J_{0,bulk} + J_{0,rear} = J_{0,\ before\ Ca/Al} + J_{0,bulk} + J_{0,metal} \tag{2}$$

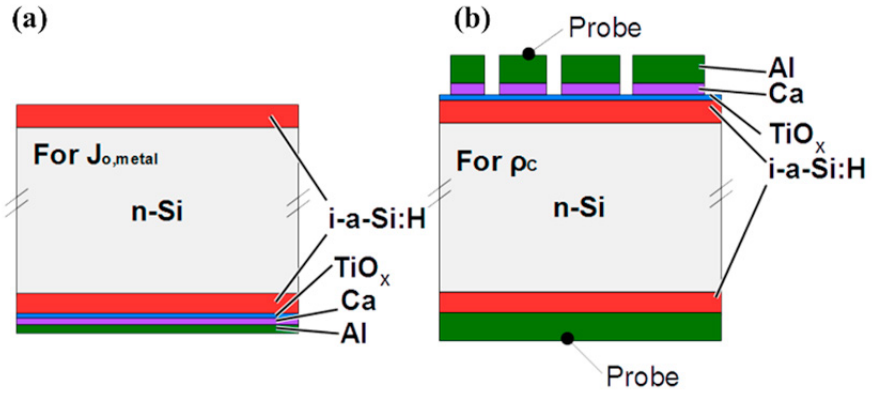

Fig. 2. (a) Sample structure for $J_{0,metal}$ measurement (b) Contact resistivity measurement sample structure.

For the measurement of ρ_C, 30 nm Ca and 170 nm Al were deposited through a shadow mask, which has differently sized dots (200 μm – 600 μm). The values of ρ_C were extracted using the two-contact-two-terminal method [11]. Total resistance is changed depending on the contact size. (Fig. 3(a)).

$$\begin{aligned} R_{Total} &= R_{C,Front} + R_{Spreading} + R_{C,Rear} + R_{Probe-wire} \\ &= \frac{\rho_C}{\pi r^2} + \frac{\rho_{Wafer}}{2\pi\pi}\tan^{-1}\left(\frac{2t_{wafer}}{r}\right) + Cons \end{aligned} \tag{3}$$

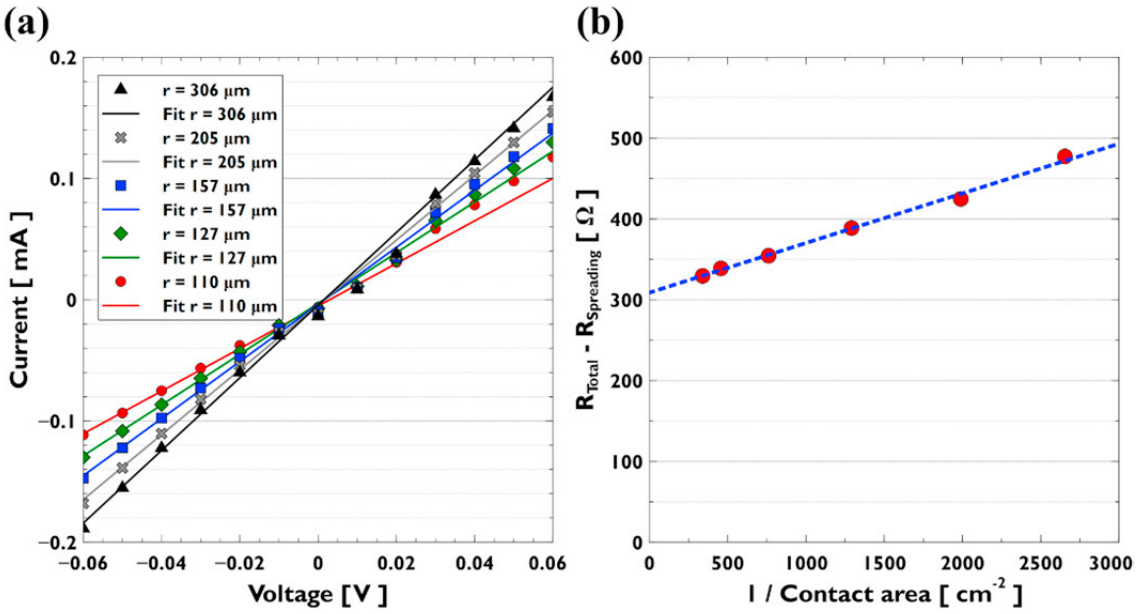

Fig. 3. ρ_C characterization. (An example of a-Si:H / TiO_X / Ca / Al) (a) IV results in various sized dots. (b) An example of slope fitting for contact resistivity evaluation.

R_{Total} is the total resistance from the IV slope and $R_{Spreading}$ is a spreading resistance which can be calculated using a front contact size, wafer resistivity (ρ_{Wafer}) and wafer thickness (t_{Wafer}). $R_{C,Front}$ is the contact resistance of a small metal dot at the front side. $R_{C,Rear}$ is the contact resistance at the rear side and $R_{Probe\text{-}wire}$ is the overall resistance caused by probe and wire of the measurement system. As shown in Fig. 3 (b), ρ_C was determined by a slope in difference between R_{Total} and $R_{spreading}$ as a function of 1 / contact area (see Eq. (3)). Consequently, the measured ρ_C comprises the ρ_C contribution of all contact layers (i-a-Si:H/TiO_X/Ca/Al). Nano scale layer structures and the chemical profile were observed through transmission electron microscopy (TEM) and energy dispersive spectroscopy (EDS) measurements in TEM measurement tool. A Keithely 4200 system was used for IV characterization.

3. Results

3.1. Ca contacts on i-a-Si:H

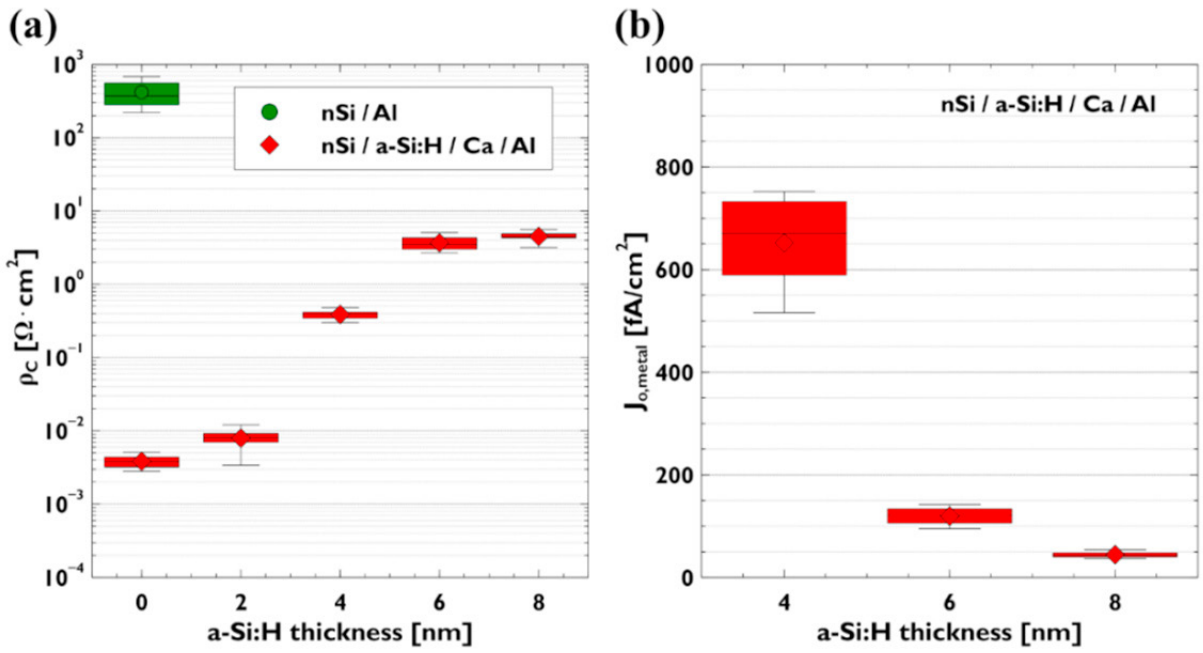

Fig. 4. (a) ρ_C dependence on a-Si:H layer thickness and metals. (b) $J_{0,metal}$ as a function of intrinsic a-Si:H thickness

As shown in Fig. 4. (a), for a metal contact directly on the substrate, an improvement in the ρc of about 5 orders of magnitude is realized by changing the metal from Al to Ca. This is a direct result of LWM on the lowly doped surface of the n-type substrate (N_D 1.8 x 10^{15} cm^{-3}). To overcome the high $J_{0,metal}$ of several thousand fA/cm^2 in Ca contact on c-Si, excellent passivation materials are required and the material band structure also needs to be considered. Taken together, i-a-Si:H is the best candidate for a good passivation and an asymmetric energy band structure. When thickness of i-a-Si:H is increased, $J_{0,metal}$ is effectively decreased and good chemical passivation was achieved from 6 nm onwards as shown in Fig. 4.(b). However, thickening i-a-Si:H increases ρ_C (Fig. 4. (a)) and a Schottky diode behavior appears for a thickness of more than 4 nm. So, although the contact passivation is greatly improved by increasing i-a-Si:H layer thickness, the low conductivity of i-a-Si:H results in an unacceptable increase of ρ_C for thick layers.

3.2. Ca based ATOM contact

Since the number of a-Si:H surface states is of similar order of magnitude to c-Si, a strong $E_{F,metal}$ pinning effect occurs on the a-Si:H surface. To suppress this effect, a MIS contact structure can be a good alternative. ρ_C is significantly changed by an interfacial layer thickness in a range of a few nm [3,4,12]. Accordingly, various thicknesses of an interfacial TiO_X layer were tested to find an optimum point which shows the lowest ρ_C. The nominal TiO_X thickness of 2 nm from quartz crystal monitor tooling factor in e-beam evaporation tool resulted in the thickness of 1.8 nm (from TEM measurement) and i-a-Si:H was conformally covered by TiO_X (see Fig. 6. (a)).

As shown in Fig. 5. (a), the interfacial thin TiO_X changes. Up to the thickness of 2 nm, the dominant $E_{F,Metal}$ depinning effect of TiO_X shifts the contact behavior from Schottky contact to ohmic contact. On the other hands, a high tunneling resistance of TiO_X becomes dominant from 3 nm onwards, and it leads to a high ρ_C and Schottky contact behavior. This trend is very similar to the previous studies [8,12]. When an optimum TiO_X interfacial layer was applied to a Ca based ATOM contact, ρ_C decreased about 2 orders of magnitude with increased $J_{0,metal}$ as shown in Fig. 5 (b). Without any n+ layer, a ρ_C of 59 $m\Omega \cdot cm^2$ and $J_{0,metal}$ of 143 fA/cm^2 were achieved.

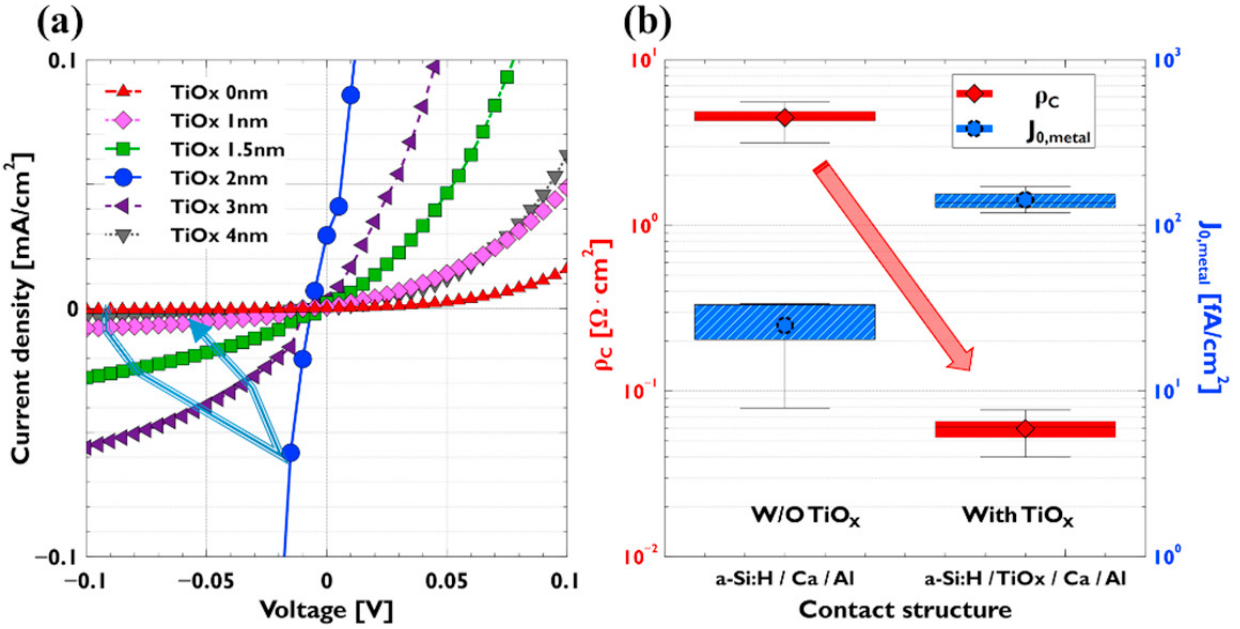

Fig. 5. (a) Interfacial TiO_X layer thickness effect on current flow. (b) Contact performance comparison of ρ_C and $J_{0,metal}$ with/without interfacial TiO_X layer.

As shown in Fig. 6. (a), very thin bright layer, SiO_X, can be found between a-Si:H and TiO_X. The SiO_X layer may be grown by O_2 in air, O_2 gas flow during the TiO_X evaporation and bonding change due to stronger Si-O bonding energy than Ti-O [13]. According to the literature [14,15], surface oxidation of a-Si:H increases defect density. However, no significant difference of effective minority carrier lifetime was between control and O_2 exposed sample in a e-beam evaporation chamber (not illustrated in this work). And attenuated total reflection fourier transform infrared spectroscopy (ATR-FTIR) was measured to observe the absorption peak ratio differences [16,17] of Si-H, $Si-H_2$, $Si-H_3$ between a-Si:H / c-Si and TiO_X / a-Si:H / c-Si samples. Also no significant difference could be found in this case (not illustrated in this work). Also, Fig. 6 (b) clearly shows that a crystallization of i-a-Si:H and TiO_X did not occur after thermal Ca / Al evaporation. Not only a-Si:H but also an amorphous phase of TiO_X is important to passivate the silicon surface [18]. Based on these data, it is reasonable to infer that $J_{0,metal}$ degradation stems mainly from e-beam induced radiation damage in i-a-Si:H like shown in other cases [19,20].

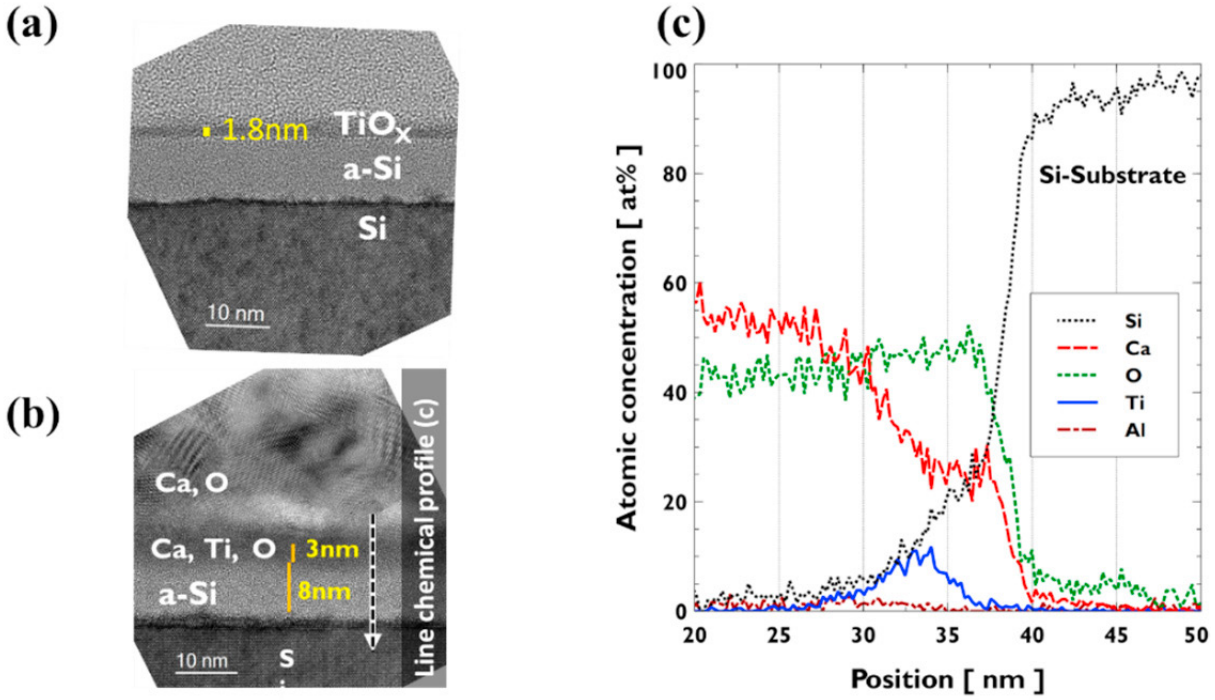

Fig. 6. (a) TEM image of TiO_X / a-Si:H / c-Si sample. (b) TEM image of Ca based ATOM contact structure. (c) Line chemical profile of ATOM contact from Ca to Si substrate (data from EDS measurement in TEM measurement tool).

As shown in Fig. 6. (b), (c), TiO_X is mixed with Ca, O, Si. These other components in TiO_X may change the properties of TiO_X. By measuring IV at 77 K, thermionic emission of electrons can be minimized and it helps to investigate an energy barrier status. In Fig. 7. (a), an ohmic contact of Ca on c-Si at room temperature is also changed to a Schottky contact at 77 K despite a Ca workfunction of 2.9 eV. This could be another clear evidence of the $E_{F,metal}$ pinning effect on a c-Si surface. An i-a-Si:H insertion between c-Si and Ca reduces the reverse current density because of a higher E_C position than the one of c-Si (see Fig. 1. (b)) and low conductivity of the a-Si:H. In the IV result of the ATOM contact at 77 K, a higher reverse current density from - 0.63 V backwards is shown than without TiO_X contact (nSi / a-Si:H / Ca / Al). Moreover, there are two levels of saturation current density since electrons cross two energy barriers, which are at the interfaces of $E_{F,Ca}$ / $E_{C,TiOx}$ and $E_{C,TiOx}$ / $E_{C,a\text{-}Si:H}$. Therefore, we could infer that TiO_X functions as a $E_{F,metal}$ depinning effect and also as an energy buffer between a-Si:H and Ca.

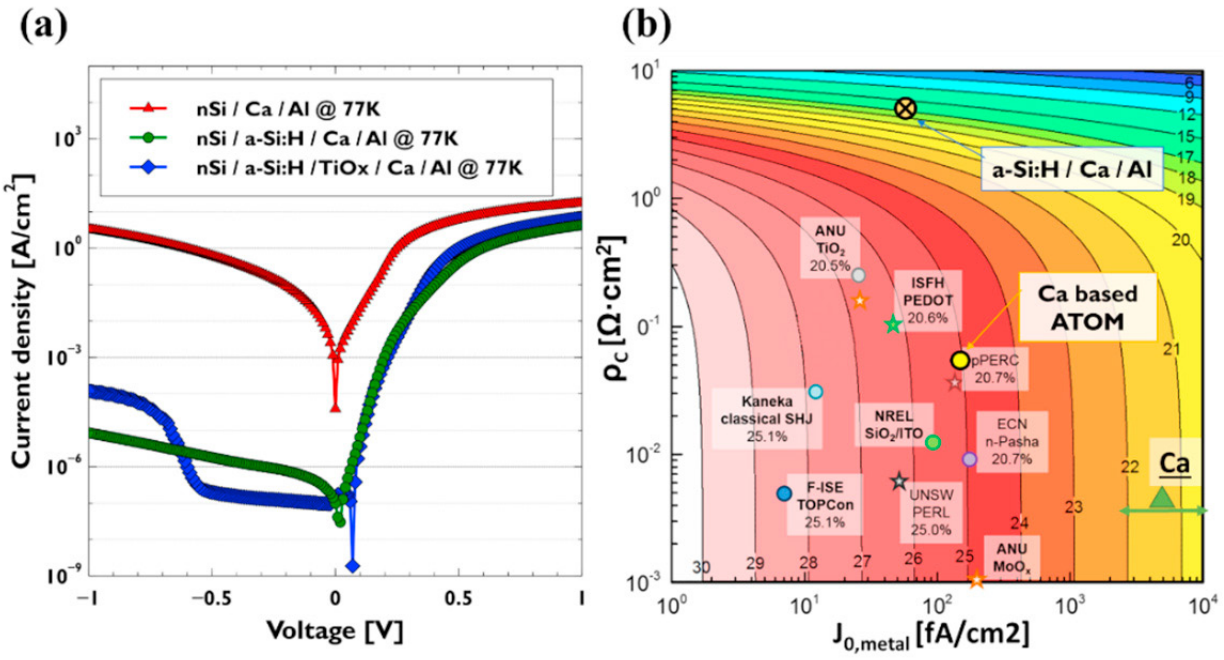

Fig. 7. (a) IV characteristics of different contact structure at low temperature (77 K). (b) Calculated potential upper limit solar cell efficiency featuring a full area contact based on ρ_C and $J_{0,metal}$ [21].

To check the potential of the developed contact, the potential efficiency limit of each contact is compared in Fig. 7 (b) [21]. The marked $J_{0,metal}$ and ρ_C were calculated assuming that the cell had a full area contact, and no other recombination (surface nor bulk), no shunting and no optical losses are considered in an efficiency of the contour plot. Although Ca on c-Si and a-Si:H / Ca are tackled by unwelcomed high $J_{0,metal}$ or high ρ_C, Ca based ATOM shows a huge potential by attaining a high limit efficiency of 25% thanks to a balance in $J_{0,metal}$ and ρ_C.

4. Conclusion

In summary, this work demonstrates the potential of a Ca based ATOM contact and how the principle of $E_{F,metal}$ depinning can be applied for silicon solar cells. The insertion of the TiO_X drastically reduces the ρ_C by two orders of magnitude. On the other hand, the contact passivation is at the moment still suffering from the TiO_X deposition. Eventually, the ATOM contact is a very promising way to achieve a low ρ_C and a low $J_{0,metal}$ for doping free solar cells.

Acknowledgements

The authors gratefully acknowledge the financial support of imec's industrial affiliation program for Si-PV. And part of this project has received funding from the European Union's Horizon 2020 research and innovation programme under the Marie Sklodowska-Curie grant agreement No 657270.

References

[1] Louwen A, Van Sark W, Schropp R, Faaij A. A cost roadmap for silicon heterojunction solar cells. Sol Energy Mater Sol Cells 2016; 147:295–314.

[2] Nishimura T, Kita K, Toriumi A. Evidence for strong Fermi-level pinning due to metal-induced gap states at metal/germanium interface. Appl Phys Lett 2007; 91:89–92.

[3] Yu H, Schaekers M, Barla K, Horiguchi N, Collaert N, Thean AVY, De Meyer K. Contact resistivities of metal-insulator-semiconductor contacts and metal-semiconductor contacts. Appl Phys Lett 2016; 108 : 171602.
[4] Jiseok K, Oldiges PJ, Hui-feng L, Niimi H, Raymond M, Zeitzoff P, Kamineni V, Adusumilli P, Chengyu N, Chafik F. Specific contact resistivity of n-type Si and Ge M-S and M-I-S contacts. 2015 Int. Conf. Simul. Semicond. Process. Devices, IEEE, 2015; 234–237.
[5] Bullock J, Hettick M, Geissbühler J, Ong AJ, Allen T, Sutter-Fella CM, Chen T, Ota H, Schaler EW, De Wolf S, Ballif C, Cuevas A, Javey A. Efficient silicon solar cells with dopant-free asymmetric heterocontacts, Nat Energy 2016; 1: 15031.
[6] Allen TG, Bullock J, Zheng P, Vaughan B, Barr M, Wan Y, Samundsett C, Walter D, Javey A, Cuevas A. Calcium contacts to n-type crystalline silicon solar cells. Prog Photovoltaics Res Appl 2016.
[7] Wronski CR, Carlson DE. Surface states and barrier heights of metal-amorphous silicon schottky barriers. Solid State Commun 1977; 23:421–424.
[8] Agrawal A, Lin J, Barth M, White R, Zheng B, Chopra S, Gupta S, Wang K, Gelatos J, Mohney SE, Datta S. Fermi level depinning and contact resistivity reduction using a reduced titania interlayer in n-silicon metal-insulator-semiconductor ohmic contacts. Appl Phys Lett 2014; 104
[9] Yang X, Bi Q, Ali H, Davis K, Schoenfeld WV, Weber K. High-Performance TiO 2 -Based Electron-Selective Contacts for Crystalline Silicon Solar Cells. Adv Mater 2016; 28: 5891–5897.
[10] Richter A, Glunz SW, Werner F, Schmidt J, Cuevas A. Improved quantitative description of Auger recombination in crystalline silicon. Phys Rev B 2012; 86:165202.
[11] Schroder DK. Material and Device Semiconductor Material and Device Third Edition; 2006.
[12] Agrawal A, Lin J, Zheng B, Sharma S, Chopra S, Wang K, Gelatos A, Mohney S, Datta S. Barrier height reduction to 0.15eV and contact resistivity reduction to 9.1×10−9 Ω-cm^2 using ultrathin TiO_2−x interlayer between metal and silicon. VLSI Technol (VLSIT), 2013 Symp, 2013; T200–T201.
[13] Luo YR. Comprehensive Handbook of Chemical Bond Energies. CRC Press; 2007.
[14] Street RA, Knights JC. Oxidation and interface states in a-Si: H. Philos Mag Part B 1981; 43:1091–1098.
[15] Winer K, Ley L. Effects of oxidation on surface band-gap states in a -Si:H. Phys Rev B 1988; 37: 8363–8369.
[16] Burrows MZ, Das UK, Opila RL, De Wolf S, Birkmire RW. Role of hydrogen bonding environment in a-Si:H films for c-Si surface passivation. J Vac Sci Technol A Vacuum Surfaces Film 2008; 26:683–687.
[17] Fujiwara H, Kondo M. Real-time monitoring and process control in amorphous/crystalline silicon heterojunction solar cells by spectroscopic ellipsometry and infrared spectroscopy. Appl Phys Lett 2005; 86:32112.
[18] Richards BS, Cotter JE, Honsberg CB. Enhancing the surface passivation of TiO2 coated silicon wafers. Appl Phys Lett 2002; 80:1123–1125.
[19] Kopp J, Warta W, Aberle A, Glunz S, Knobloch J. Impact of metallization techniques on 20 % efficient silicon solar cells. 22nd IEEE Photovolt Spec Conf, 1991; 278–283.
[20] Klaver A. Irradiation-induced degradation of amorphous silicon solar cells in space. Eindhoven Univeristy of Technology; 2007 p. 75-117.
[21] Van de Loo BWH. Atomic-Layer-Deposited surface passivation schemes for silicon solar cells. Eindhoven University of Technology; 2017 p. 63.